SEDIMENTOLOGY the journal of the International Association of Sedimentologists IAS

Sedimentology (2026) doi: 10.1111/sed.70143

Not all rhodoliths need a bed–depositional mechanisms in shallow water *Sporolithon nodosum* rhodoliths from the Whangaparaoa peninsula (North Island, New Zealand)

SEBASTIAN TEICHERT*, THOMAS MÖLG†, INES PYKO*, ELENA KROPAČ†, PETER MARRIOTT‡, ROBERTA D'ARCHINO‡, NICOLAS CULLEN§, DANIELA BASSO¶, NORA PERSCH*, SVEN BACH*, ELLA LIS**, BEAU MASTERS** and WENDY NELSON**,††

**Lehrstuhl für Paläoumwelt, GeoZentrum Nordbayern, Friedrich-Alexander-Universität Erlangen-Nürnberg (FAU), Loewenichstraße 28, 91054 Erlangen, Germany (E-mail: sebastian.teichert@fau.de)*

†Climate System Research Group, Institute of Geography, Friedrich-Alexander-Universität Erlangen-Nürnberg (FAU), Erlangen, Germany

‡Earth Sciences New Zealand, Private Bag 14901, Kilbirnie, Wellington, New Zealand

§School of Geography, University of Otago, Dunedin, New Zealand

¶Department of Earth and Environmental Sciences, University of Milano-Bicocca, Piazza della Scienza 4, Milano 20126, Italy

***School of Biological Sciences, University of Auckland, Auckland, New Zealand*

††Natural Sciences Department, Auckland Museum Tāmaki Paenga Hira, Auckland, New Zealand

Associate Editor: Jody Webster

ABSTRACT

Rhodoliths, formed by crustose coralline algae (CCA), are prominent components in carbonate platform deposits, contributing to the characteristic rhodalgal facies. Their formation is influenced by both biological and physical factors, and under specific conditions, they can accumulate, forming extensive rhodolith beds. This study examines the depositional mechanisms underlying the formation of monospecific (*Sporolithon nodosum*) shallow-water rhodoliths from the Whangaparaoa Peninsula, North Island, New Zealand. The findings suggest that these rhodoliths originate in subtidal rocky channels at approximately 5 m depth, by the encrustation of nuclei derived from surrounding geological strata. Following their formation, these rhodoliths are transported into intertidal channel systems and eventually deposited in supratidal beach areas. Notably, the structure, morphology and composition of rhodoliths across these three depositional settings exhibit minimal variation, suggesting that the rhodoliths belong to a strongly interconnected coastal system with only brief intervals between translocation events. In this context, the study provides a sedimentological model for the development of rhodoliths in a coastal setting. Furthermore, it challenges the presence of a significant rhodolith bed *sensu stricto* in deeper offshore waters, as exploratory diving surveys revealed extensive sand deposits that hinder rhodolith development in these areas.

Keywords Crustose coralline algae, New Zealand, non-geniculate coralline algae, rhodolith formation, rhodoliths, *Sporolithon nodosum*, Whangaparaoa peninsula.

INTRODUCTION

Coralline algae of the subclass Corallinophycidae Le Gall & Saunders, 2007 are heavily calcifying benthic macroalgae that are distributed globally (Foster, 2001; Teichert, 2024), including the polar areas on both hemispheres (López Correa *et al.*, 2023; Teichert *et al.*, 2024) and which have a fossil record dating back to Palaeozoic ages (Riding *et al.*, 1998; Teichert *et al.*, 2019). Non-geniculate coralline algae, frequently referred as crustose coralline algae (CCA) have an extensive bathymetric range and are found in diverse habitats such as shallow reef crests (Dean *et al.*, 2015), tidal pools (Nalin *et al.*, 2008) and even at depths of up to 268 m, representing the deepest known occurrence of plant life on Earth (Littler *et al.*, 1985). Moreover, there are first records of CCA inhabiting freshwater environments (Žuljević *et al.*, 2016; Ragazzola *et al.*, 2020). CCA have a great phenotypic plasticity and the same species may form crusts fixed to bedrock or large boulders, but can also occur free-living in the form of so-called rhodoliths, also referred to as maërl (Bosence, 1983b). However, the scientific term rhodolith is preferred to the vernacular term maërl (Basso *et al.*, 2016). Rhodoliths can form extensive accumulations, giving rise to the so-called rhodolith beds. Rhodolith beds play a vital role in both ecological and sedimentological processes within the ocean, due to their properties as ecosystem engineers (Kamenos *et al.*, 2004; Teichert, 2014; Straube *et al.*, 2024; Tâmega *et al.*, 2024), their massive calcium carbonate skeletons and their wide distribution (Tuya *et al.*, 2023). Currently there is no unifying definition of a rhodolith bed in terms of coverage and proportion of living compared to dead rhodoliths (Bulleri *et al.*, 2025). However, different studies have used varying criteria, such as a cover of living coralline thalli greater than 10% (Steller *et al.*, 2003; Basso *et al.*, 2016) or 30% (OSPAR, 2008), within an area of at least 100 m^2 (Rinde *et al.*, 2022) or 500 m^2 for the purpose of mapping at the regional scale and for international initiatives of habitat mapping (Basso *et al.*, 2016).

Our study describes rhodolith accumulations from the Whangaparaoa peninsula located in the North Island of New Zealand and establishes a new depositional framework for their formation and development, hypothesising that the Whangaparaoa rhodolith system represents a spatially restricted and dynamically connected coastal accumulation rather than a deposit primarily supplied by a large offshore rhodolith bed. The site has been analysed before (Nalin *et al.*, 2008; Basso *et al.*, 2009) and the rhodolith production area has been estimated to be located within the intertidal and the very shallow subtidal setting, but these early studies did not provide direct evidence from subtidal exploration (Nalin *et al.*, 2008; Basso *et al.*, 2009).

Although the occurrence of isolated rhodoliths outside fully developed rhodolith beds is not unexpected, the exceptionally high abundance of rhodoliths observed in the present shallow-water setting raises the question of whether this area represents the preferential growth environment of the population. The studied habitat is characterised by strong hydrodynamic disturbance, including tidal currents, storm influence, repeated overturning, abrasion and episodic transport processes, all of which indicate a highly dynamic and potentially unstable environment for sustained rhodolith growth. Basso *et al.* (2009) interpreted the Whangaparaoa rhodoliths as developing under conditions of frequent hydrodynamic disturbance, reflected by their compact internal structure, apical abrasion, intercalary regrowth after breakage and multiple abrasion surfaces separating successive growth phases. While such settings may facilitate local accumulation and temporary preservation of rhodoliths, we hypothesise that the preferential growth zones of the rhodolith population may primarily occur in deeper and more stable subtidal environments, potentially including true rhodolith-bed settings, from which rhodoliths are episodically transported or redistributed into the extremely shallow-water environment.

This interpretation also highlights an important difference between rhodoliths and reef-forming corals. Solitary coral colonies outside reef frameworks are relatively unsurprising because many scleractinian corals disperse via planktonic planula larvae capable of surviving transport over considerable distances before settlement (Richmond & Hunter, 1990). Rhodolith-forming coralline algae, by contrast, lack such a larval dispersal stage and instead propagate through spores and vegetative fragmentation, indicating rather limited dispersal capacities for CCA (Pardo *et al.*, 2019).

Our study includes the supratidal, intertidal and subtidal environments (1 to 17 m water

depth) around Army Bay in order to test the hypothesis that the principal production area of the rhodoliths is located within the shallow rocky subtidal zone or an offshore rhodolith bed rather than within the highly dynamic intertidal environment itself. To evaluate this hypothesis, rhodoliths from all depositional settings were quantitatively compared with regard to morphology, internal composition, preservation state and lithoclastic nuclei.

Morphometric analyses of rhodolith size, weight, sphericity and shape were conducted to evaluate hydrodynamic sorting processes and potential transport pathways between the subtidal, intertidal and supratidal zones. In particular, the occurrence of smaller and lighter rhodoliths within the supratidal settings was analysed to test whether selective landward transport affects rhodolith distribution across the coastal profile. The supratidal accumulations furthermore consist predominantly of dead and bleached rhodoliths, suggesting terminal depositional environments rather than active growth settings.

To test whether rhodoliths from the different environments represent separate in situ populations or instead belong to a single interconnected transport system, internal rhodolith compositions were quantitatively analysed via micro-computed tomography (μCT). These analyses focused on the relative abundance of skeletal contributors and bioerosional structures within the rhodolith matrix. Comparable internal compositions across all investigated settings would support repeated redistribution of the same rhodolith population rather than independent local formation. Likewise, petrographic analyses of lithoclastic rhodolith nuclei were carried out to determine whether rhodolith nuclei from the different depositional environments share a common geological source related to the adjacent Miocene flysch deposits exposed at Army Bay.

In addition, wave stress and prevailing wave directions were analysed to evaluate whether modern hydrodynamic conditions are capable of driving the proposed onshore-directed rhodolith transport from the rocky shallow subtidal zone into intertidal channels and supratidal beach deposits. Offshore subtidal areas around Army Bay and Tiritiri Matangi Island were furthermore surveyed regarding the occurrence of rhodolith beds *sensu stricto* and their possible connection to the nearshore rhodolith system.

The combined results are used to establish an updated sedimentological model for the formation, transport and redistribution of shallow-water rhodoliths within a spatially restricted but highly dynamic coastal environment.

STUDY SITE

The working area (36°35.92′ S, 174°48.91′ E) is located in Army Bay, on the northern coast of the Whangaparaoa Peninsula and around Tiritiri Matangi Island, North Island of New Zealand (Fig. 1A to C). The Whangaparaoa Peninsula is an east–west-oriented headland extending for about 12 km into the western Hauraki Gulf, north of Auckland. The Hauraki Gulf is sheltered from the Southern Ocean, but storm events are known to produce significant wave stress (Gorman *et al.*, 2003). The tidal ranges in the Hauraki Gulf show large local variation: the mean tidal range at Army Bay is 2.18 m (Walters *et al.*, 2001).

The studied transitional area lies between the intertidal zone and open sea, paralleling the coastline for about 300 m and is about 100 m in width (Fig. 1D). The geology of the study area is characterised by deformed turbidites and syn-sedimentary slides of the tectonically active Waitemata Basin (Spörli & Rowland, 2007). At Army Bay, the coastal cliff of the peninsula is fronted by a marine abrasion platform which cuts on the deformed Miocene flysch deposits (Fig. 1E), mainly consisting of turbidites and volcanoclastic grit (Ballance, 1974; Spörli & Rowland, 2007; Basso *et al.*, 2009). This platform is dissected by numerous channels 0.5 to 2 m in width, which connect several tidal pools up to 10 m in diameter. These structures carve into the thick volcanoclastic debris flows, the so-called Parnell Grit beds, within the bedded flysch of the Waitemata Group (Allen, 2004; Nalin *et al.*, 2008). The pools and channels covered by 30 to 50 cm of seawater at low tide (Fig. 1F and G) have been identified before as the potential production site of rhodoliths by Nalin *et al.* (2008). The channelled flysch deposits continue in the subtidal areas, stepwise progressing to about 5 m water depth (Fig. 1H) and further work by Basso *et al.* (2009) already indicated the shallow subtidal zone as potential main site of production, with survival occurring also in the intertidal channels.

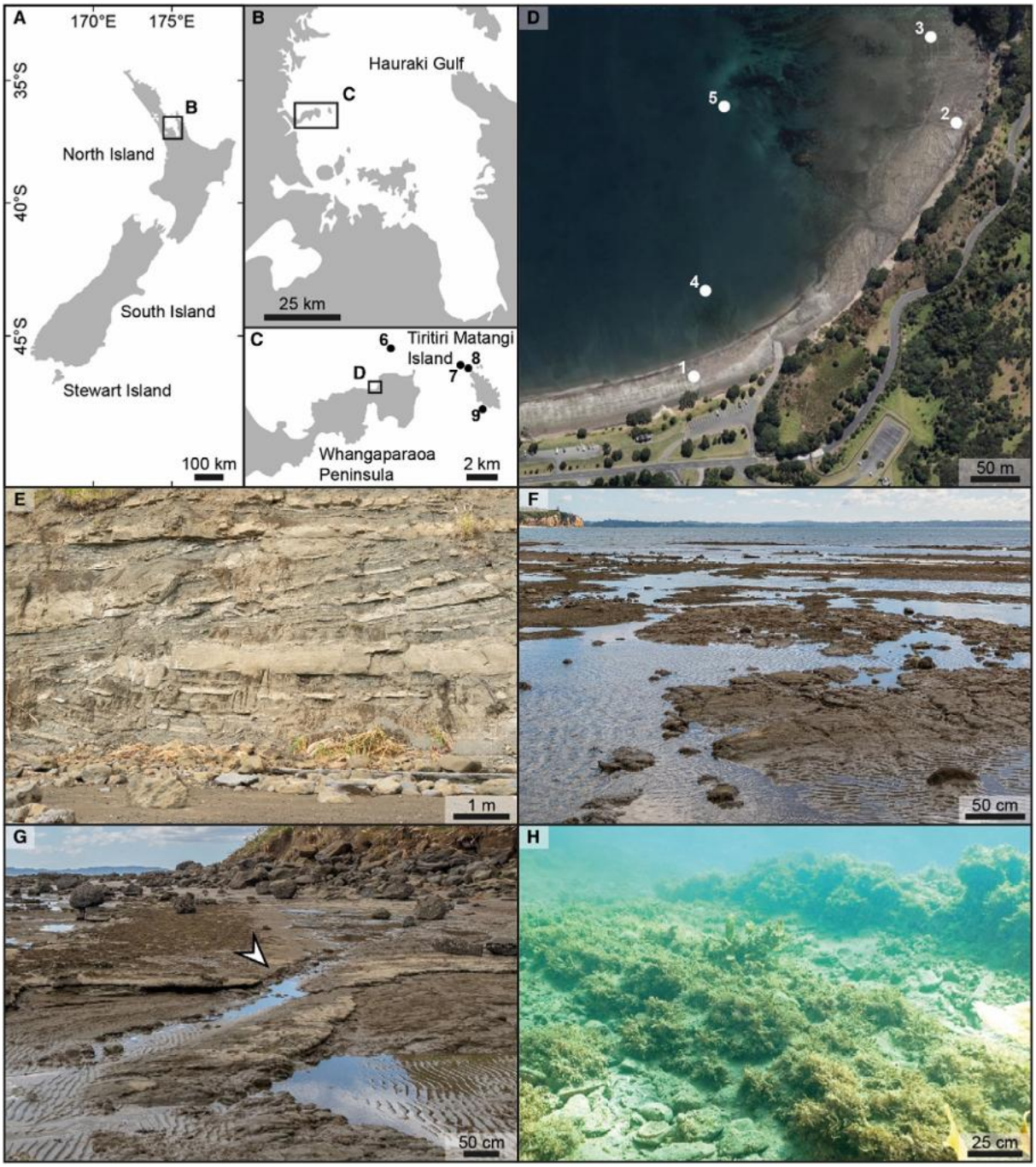

Fig. 1. Working area and site description. (A) Map of New Zealand, working area is located on the North Island; area in the rectangle shown in B. (B) Schematic map of the Hauraki Gulf; area in the rectangle shown in C. (C) Schematic map of the Whangaparaoa Peninsula and Tiritiri Matangi Island; numbered black dots indicate positions of scuba dive sampling spots (see also Table 1); area in the rectangle shown in D. (D) Satellite image (courtesy of Google Inc.) of Army Bay; numbered white dots indicate snorkelling and hand collection sampling spots (see also Table 1). (E) Section of the coastal cliff at Army Bay, featuring Miocene flysch deposits mainly consisting of turbidites and volcanoclastic grit. (F) Tidal pools at Army Bay with 30 to 50 cm water depth during low tide with living rhodoliths inside. (G) Typical channel (white arrow) arising from the flysch deposits, containing living rhodoliths. (H) Channelled flysch deposits continuing in the subtidal areas, stepwise progressing to about 5 m water depth and identified as the actual main areas of rhodolith formation.

METHODS

Site descriptions and rhodolith collection

Rhodoliths were collected on March 22 and 23 in 2023. All collected specimens were deposited at GeoZentrum Nordbayern, Friedrich-Alexander-Universität Erlangen-Nürnberg (FAU). The rhodolith-bearing tidal pools were accessible during low tide and live rhodoliths were collected by hand (sites 1 to 3). Dead, bleached rhodolith specimens were also collected from the supratidal rocky and sandy shore areas. The subtidal areas up to 5 m water depth at Army Bay were inspected and rhodoliths were collected by snorkelling (sites 4 to 5). Underwater video footage and photography were conducted using a Sony Digital Single-Lens Reflex (DSLR) camera in a waterproof housing. Deeper offshore waters around Army Bay were examined by scuba diving (sites 6 to 9) from a small research vessel and rhodolith specimens were collected by hand. All site categories and the relevant sampling data are summarised in Table 1. Using photograph and video data as well as the personal observations from the collectors, the sites are described including substrate availability for potential rhodolith formation.

Morphological and anatomical description of rhodoliths

Rhodoliths collected for this study include both rhodoliths *sensu stricto*, where the CCA skeleton makes up >50% of the whole structure (Steneck, 1986) as well as CCA-coated grains (Teichert, 2024). Altogether 103 rhodoliths were collected, 74 of which were alive upon sampling as they were pink-coloured at least on a portion of their surface. The dead and bleached specimens derived completely from the sandy and rocky supratidal collections. After collection, rhodoliths were air-dried for 7 days, stored in sealed plastic bags and sent to FAU Erlangen-Nürnberg for further analysis.

To compare the dimensional characteristics of rhodoliths from all sampling sites in order to allow for conclusions on potential interconnections between these sites, the specimens' long (L), intermediate (I) and short (S) axes were measured. For visual comparison, results were plotted into a pebble-shape diagram according to Sneed & Folk (1958) using Triplot (Graham & Midgley, 2000).

Rhodolith sphericity was analysed by applying the maximum projection sphericity equation:

Table 1. Information on rhodolith sampling sites, sorted from supratidal to deep waters.

Site number	Site name	Site category	Collection method	Rhodoliths collected [n]	Lat. S [DD]	Long. E [DD]	Water depth [m]
1	Army Bay	Beach supratidal	Hand collection	9	−36.601	174.813	0
2	Army Bay	Rocky supratidal	Hand collection	19	−36.599	174.816	0
3	Army Bay	Rocky intertidal	Hand collection	18	−36.598	174.816	0.1
4	Army Bay	Sandy subtidal	Snorkelling	9	−36.600	174.813	1.5
5	Army Bay	Rocky subtidal	Snorkelling	33	−36.599	174.813	1.0 to 5.0
6	Wellington Rocks	Sandy subtidal	Scuba diving	8	−36.584	174.823	11.6
7	Whangaparaoa Passage	Sandy subtidal	Scuba diving	5	−36.590	174.876	13.7
8	Bollons Rock	Sandy subtidal	Scuba diving	1	−36.591	174.877	15.8
9	Tiritiri Matangi Island	Sandy subtidal	Scuba diving	1	−36.610	174.891	16.6

$$\text{Sphericity} = \sqrt[3]{\frac{S^2}{LI}} \quad (1)$$

as described in Sneed & Folk (1958). Rhodolith size was estimated by calculating the volume of an ellipsoid via the equation:

$$\text{Volume} = \sqrt{\frac{LIS}{4\pi}} \quad (2)$$

as described in Bosence (1976). Rhodolith weight was measured via a precision balance.

Specifying the collection sites 1 to 9 as groups, non-parametric (not all data were normally distributed) one-way PerMANOVA (permutational multivariate analysis of variance) with a Bray–Curtis similarity index and 10 000 permutations was used to account for significant differences between sites, accounting for variations in rhodolith sphericity, size and weight. Pairwise comparisons (*post hoc*) were corrected via sequential Bonferroni significance. Results were also visualised by combined jitter- and boxplots.

For the description of specimen morphology and anatomy, rhodoliths were photographed with a Nikon DSLR camera at various magnifications and analysed via optical and scanning electron microscopy (SEM). For optical microscopy, rhodoliths were embedded in resin, cut with a water-cooled, low-speed rock diamond saw and ground the surface on water-cooled diamond plates with 120, 240, 400 and 800 grit. Surfaces were then mounted to glass plates and thinned to 30 microns. Thin sections were then analysed with transmitted light with a Zeiss Axio Imager.M2m and Axio Zoom.V16 via the Zeiss ZEN software. For SEM, specimens were split with a bench vice and mounted on aluminium stubs using wood glue and sputter coated with gold under argon gas for 6 min using 2-min intervals with 30-s breaks at 40 mA and 10 000 V. Samples were then examined with a Tescan Vega 2 xmu SEM at 25 kV.

Interior rhodolith composition analysis via µCT

As the study hypothesises that the main area of rhodolith production is the rocky subtidal zone of Army Bay (site number 5), the inner compositions of 10 rhodoliths were compared, two from the sandy subtidal zone (site 4, samples NZ-166, NZ-174), three from the rocky subtidal zone (site 5, samples NZ-106, NZ-109, NZ-126) and five from the beach supratidal zone (site 1, samples NZ-175, NZ-176, NZ-179, NZ-181, NZ-183). For this analysis, virtual cross-sections of rhodoliths from each site were generated using micro-computed X-ray tomography (µCT). This advanced imaging technique enabled the non-destructive analysis of rhodoliths while allowing for the creation of an unlimited number of cross-sections in various orientations. The ability to obtain multiple virtual cross-sections provided a comprehensive and detailed visualisation of each rhodolith's internal structure. Scanning was performed using a General Electric (GE)/Phoenix v|tome|x S 240 (GE/Phoenix, Wunstorf, Germany) micro-CT scanner. To reduce beam hardening effects, a 0.5-mm copper filter was applied during the scanning process. Scanning parameters, including voltage, current, field-object distance (FOD), voxel size and field-detector distance (FDD), were optimised for each sample manually. Data reconstruction was performed using the Feldkamp algorithm, implemented via the GE/Phoenix software datos 4 (GE/Phoenix, Wunstorf, Germany). Post-processing was carried out using VolumeGraphics software, which facilitated the generation of thin sections and the virtual segmentation of each sample into vertical cross-sections for further analysis. This approach yielded high-resolution images of the rhodoliths' internal structures, enabling detailed examination of their composition and morphological features. The taxonomic groups of the calcareous matrix that could be identified according to their distinct skeletal structures (Flügel, 2010; Pyko *et al.*, 2025) within the virtual cross-sections were CCA, bryozoans, balanids, geniculate coralline algae, serpulids and boring bivalves. Moreover, it was possible to identify bioerosional features based on their shape and size. To estimate quantitatively if the inner rhodolith compositions from the various sites differ significantly, the point-counting method was employed, using approximately 300 points per rhodolith sample and the categories (i) crustose coralline algae (CCA), (ii) bryozoans, (iii) balanids, (iv) bioerosion, (v) serpulids and (vi) boring bivalves. A grid step size of 2 mm was determined by the smallest rhodolith to ensure the counts of 300 points. One complete rhodolith represented a single sample and to achieve enough points, a varying number of cross-sections per rhodolith, according to its size, was counted. The number of cross-sections counted has no impact on the results, if the

distance between the points is the same. Specifying the collection sites as groups, a one-way PerMANOVA with a Bray–Curtis similarity index and 10 000 permutations was used to account for significant differences between sites. Results were also visualised by stacked bar plots.

Petrographic analysis of lithoclastic rhodolith nuclei

As an additional method to test the hypothesis that the main area of rhodolith production is the rocky subtidal zone of Army Bay (site number 5), the petrographic features of rhodolith nuclei from three different sites (sandy subtidal of Wellington Rocks, site 6, sample number NZ-154; sandy subtidal of Army Bay, site 4, sample number NZ-171; rocky supratidal of Army Bay, site 2, sample number NZ-192) were compared with the petrographic features of two lithoclasts (samples NZ-Lith-1 and NZ-Lith-2) collected from the coastal cliffs featuring the deformed Miocene flysch deposits that are characteristic for this area.

For petrographic analysis via optical microscopy, thin sections were prepared as described above. Thin sections were then analysed with transmitted light with a Zeiss Axio Imager.M2m and Axio Zoom.V16 via the Zeiss ZEN software. To estimate quantitatively if the petrographic features of rhodolith nuclei and lithoclasts differ significantly, the point-counting method was employed based on the cell model method as described by Demirmen (1971). Regarding cell size, squares of 2 mm edge length were chosen and a 0.1-mm grid spacing was used. As component categories, quartz, feldspar, cement, bioclast, silt, volcanic ash and 'unspecified' were used. Specifying rhodolith nuclei as group 1 and lithoclasts as group 2, a one-way PerMANOVA with a Bray–Curtis similarity index and 10 000 permutations was used to account for significant differences between sites. Results were also visualised by stacked bar plots. Moreover, the sedimentological features in the thin sections were analysed to account for between sample similarities.

Estimation of wave stress

For the estimation of wave stress in Army Bay to evaluate its role in potential rhodolith transport, the ERA5 dataset (Hersbach *et al.*, 2020) was used on a monthly resolution over a time interval of 30 years (1994 to 2023). Data were interpolated for −36.59° N, 174.8° E and the following variables were used to produce an overview on the wave regime prevailing in Army Bay: '10 m wind speed', '10 m neutral wind speed', 'ocean surface stress equivalent 10 m neutral wind speed', 'mean wave direction', 'significant height of wind waves' and 'significant height of combined waves and swell'. Wave data have a spatial resolution of 0.65°, atmospheric data have a spatial resolution of 0.25°.

RESULTS

Site descriptions and rhodolith occurrences

Altogether, rhodoliths from nine different sites around Army Bay and Tiritiri Matangi Island were collected (Table 1; Fig. 1C and D). Site 1 was a supratidal, flat beach area and featured only bleached, dead rhodoliths which were washed ashore. Site 2 was a rocky supratidal area with abraded but still visible channel structures in which bleached, dead rhodoliths accumulated. Site 3 was the intertidal area that has been described by Nalin *et al.* (2008) as the preferential growth zones of the rhodoliths. Rhodoliths were present in the pools and channels predetermined by the geological structures. The rhodoliths were half buried in a poorly sorted, sandy to pebbly sediment, rich in bioclastic debris and abraded mollusc shells. Most of these rhodoliths were alive, but bleached, dead specimens occurred as well. Site 4 was characterised as a sandy subtidal site fronting the beach area of Army Bay. Living rhodoliths occurred, but were less common than in the rocky intertidal zone of site 3. Most rhodoliths were collected at site 5, the rocky subtidal areas at Army Bay. This site can be considered as an underwater continuation of the channels at site 3. However, the channels were less abraded in this area, thus resembling the spur and groove formations of many coral reefs (Rogers *et al.*, 2015). The spurs were colonised by thick accumulations of brown algae and the rocky walls of the spurs were sometimes encrusted by CCA (Fig. 2A). The grooves function as sediment traps, contained sediments were sand to cobble sized and rich in abraded and bioeroded bioclasts as well as accumulations of living and dead rhodoliths, which sometimes were half covered by sediments (Fig. 2B and C). The areas offshore Army Bay (site 6) and around Tiritiri Matangi Island (sites 7 to 9) were mainly characterised by flat sand

Fig. 2. Subtidal rhodolith collection sites at Army Bay. (A) Spur structure of the rocky subtidal zones at site 5, tops were densely colonised with fleshy brown algae (kelp *Ecklonia radiata*, black arrow); exposed rocky areas were partly covered with encrusting CCA (white arrow). (B) Groove structure of the rocky subtidal zones at site 5 that acts as a sediment trap, including several rhodoliths (white arrows). (C) Close-up of the sediment in the groove structures at site 5, including living (red) and dead (bleached) rhodoliths; the sediment was rich in bioclasts, many of them strongly abraded and/or bioeroded. (D) Boulder accumulation on sandy subtidal substrate at site 6 offshore Army Bay, having a similar ecological function as the spur structures at site 5. The tops were densely colonised with fleshy brown algae (kelp *Ecklonia radiata*, black arrow) and the exposed rocky areas were partly covered by CCA (white arrow); rhodoliths occurred rarely.

accumulations that lacked rhodolith occurrences. Rhodoliths only appeared around larger rock accumulations, especially at sites 6 and 7. Site 6 was especially characterised by the existence of large boulder structures, which were densely colonised by brown algae and encrusting CCA under the canopy (Fig. 2D).

Rhodolith morphology

Sphericities for the five Army Bay sites were very similar, while sizes and weights for the rocky supratidal rhodoliths (site 2) were much lower than for the rest (Fig. 3A). Rhodolith sphericity for offshore Army Bay site 6 clearly differed from

Fig. 3. Summary of rhodolith morphologies from all sites. (A) Combined box and jitter plots for distribution of rhodolith sphericities, sizes and weights at all sites except for sites 8 and 9, which have only one measurement each. Note that rhodoliths from site 2 (rocky supratidal) were smaller and lighter than for the other sites. (B) Rhodolith shape distributions for each site are visualised by pebble shape diagrams according to Sneed & Folk (1958), indicating that while all Army Bay sites mainly featured compact rhodoliths, the shape distribution for the samples from sites 6 and 7 was much broader; the explanatory power for sites 8 and 9 was negligible because only one rhodolith was sampled at each site. Grey lines with values 0.2 to 0.9 represent maximum projection sphericity isolines, I, intermediate rhodolith axis; L, long rhodolith axis; S, short rhodolith axis.

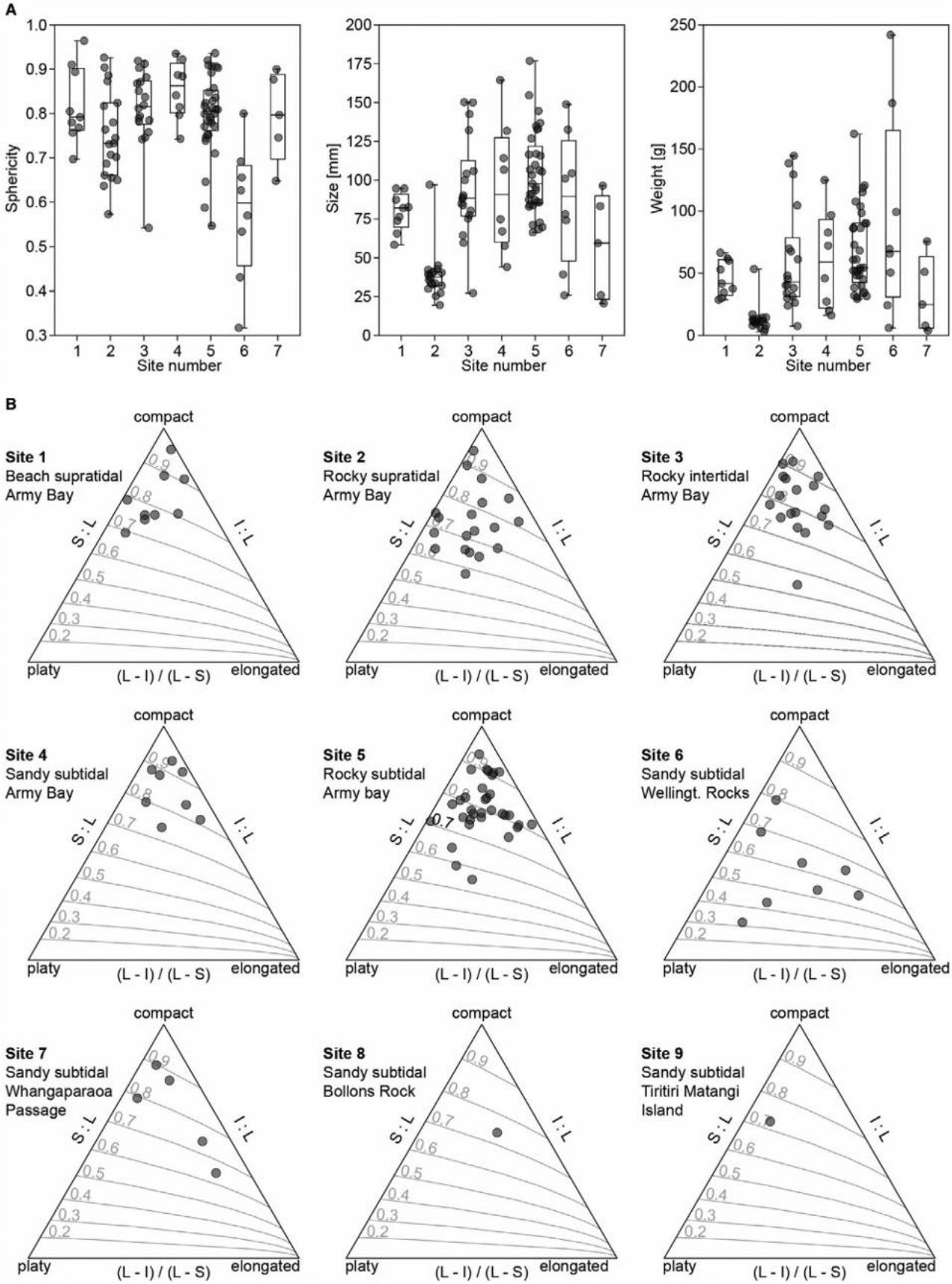

the nearshore Army Bay sites. The Tiritiri Matangi Island sites (7 to 9), must be interpreted conservatively, because sample sizes were low due to the rare rhodolith occurrences. Rhodolith shape distributions for each site were visualised by pebble shape diagrams according to Sneed & Folk (1958), indicating that while all Army Bay sites mainly featured compact rhodoliths, the shape distribution for offshore Army Bay and around Tiritiri Matangi Island was much broader (Fig. 3B). Putting all shape parameters in context, the PerMANOVA indicates significant differences between sites ($F = 12.4$, $P < 0.0001$) considering rhodolith axis lengths, sphericity, size and weight. Pairwise site comparisons (*post hoc*) corrected via sequential Bonferroni significance indicate that site 2 (rocky supratidal of Army Bay) differed significantly from the other sites Army Bay sites as well as from the sandy subtidal zone at Wellington Rocks (Table 2).

Rhodolith description and taxonomy

Molecular analyses were not conducted for all 102 specimens in the present study. However, previous DNA-based taxonomic work on New Zealand *Sporolithon* rhodoliths demonstrated that specimens formerly assigned to *S. durum* correspond to *Sporolithon nodosum* Farr & W.A. Nelson an endemic New Zealand species (Gabrielson *et al.*, 2023). In addition, previously sequenced rhodoliths from the Whangaparaoa area have consistently been assigned to this species (pers. comm. Wendy Nelson). Species identification in the present study was therefore based on diagnostic morpho-anatomical characters in combination with this existing molecular taxonomic framework. All collected rhodoliths were monospecific, consisting of the CCA *S. nodosum*, with a monomerous construction, flared epithallial cells and common cell fusions and secondary pit connections (Fig. 4A and B). Calcified compartments containing tetrasporangia were arranged in irregular shaped, raised sori (Fig. 4C). Most of the collected *Sporolithon*-rhodoliths were nucleated with the nuclei consisting of lithoclasts (see below for a detailed petrographic description). While the majority of the collected samples were rhodoliths *sensu stricto*, that is, the CCA skeleton contributes ≥50% to the overall volume of the structure, several specimens can be regarded as CCA-coated grains, where only a thin layer of CCA encrusts a nucleus. However, this differentiation does not affect the hypotheses of this study. The rhodoliths show a compact internal structure, mostly laminar concentric around the nucleus, turning into fruticose towards the surface (Fig. 4D). Many of the rhodoliths show alterations in the form of bioerosion (Fig. 4E) and abraded tips of the branches (Fig. 4F), which indicates a regular exposure to hydrodynamic stress (Basso *et al.*, 2009). Recolonisation of abraded CCA surfaces with individuals of the same species was a common feature in the sampling area and the resulting growth interruptions are clearly evident macro- and microscopically (Fig. 4G to I).

Table 2. Pairwise site comparisons (*post hoc*) corrected via sequential Bonferroni significance accounting for variations in rhodolith axis lengths, sphericity, size and weight. Differences are considered significant for $P < 0.05$, also indicated by green cells. Note that sample numbers for sites 7 to 8 are very low.

	Site 1	Site 2	Site 3	Site 4	Site 5	Site 6	Site 7	Site 8	Site 9
Site 1		0.0001	0.2597	0.3217	0.0191	0.1217	0.1398	0.7974	0.096
Site 2	0.0001		0.0001	0.0002	0.0001	0.0005	0.0508	0.1002	0.0472
Site 3	0.2597	0.0001		0.981	0.3328	0.2105	0.0736	0.8957	0.0558
Site 4	0.3217	0.0002	0.981		0.4606	0.3615	0.1468	1	0.1093
Site 5	0.0191	0.0001	0.3328	0.4606		0.1458	0.0053	0.6736	0.0299
Site 6	0.1217	0.0005	0.2105	0.3615	0.1458		0.1475	0.7826	0.1103
Site 7	0.1398	0.0508	0.0736	0.1468	0.0053	0.1475		0.8344	0.1692
Site 8	0.7974	0.1002	0.8957	1	0.6736	0.7826	0.8344		1
Site 9	0.096	0.0472	0.0558	0.1093	0.0299	0.1103	0.1692	1	

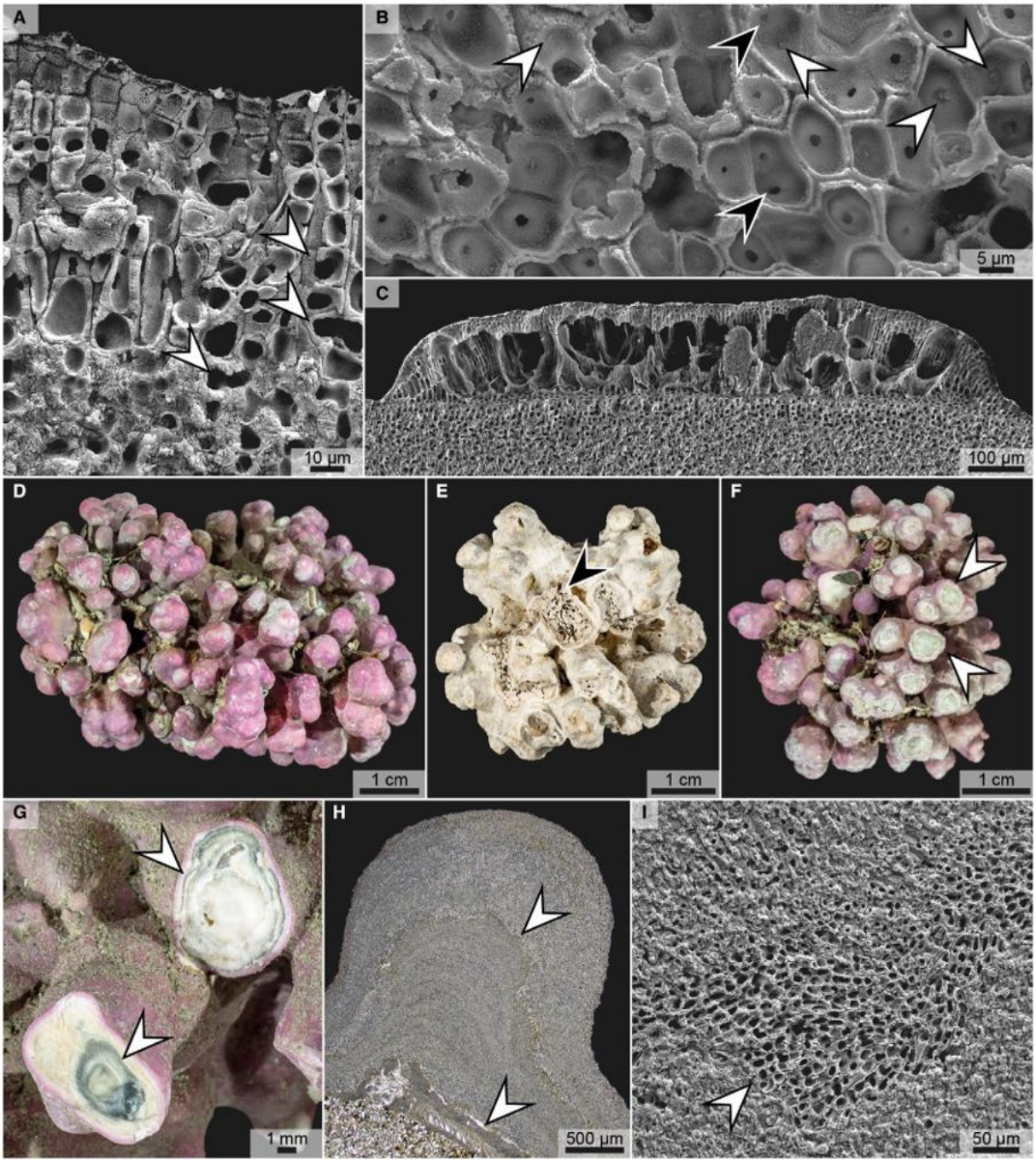

Fig. 4. Morphology and anatomy of *Sporolithon nodosum* rhodoliths; NZ-numbers in brackets indicate sample numbers of individual rhodoliths. (A) Cell fusions (white arrows) (NZ-122). (B) Primary pit connections (white arrow) and secondary pit connections (black arrow) (NZ-122). (C) Irregular shaped, raised sori (NZ-122). (D) Rhodolith (NZ-122) with compact internal structure, mostly laminar concentric around the nucleus, turning into fruticose towards the surface. (E) Dead, bleached rhodolith (NZ-183) with intense bioerosion visible at broken-off branches. (F) Rhodolith (NZ-132) with abraded branch tips (white arrows) as evidence for frequent movement. (G) Growth interruption visible as dark-coloured rims (white arrows) at broken-off branches (NZ-148). (H) Several generations of growth interruptions (white arrows) visible in a thin section, note the heavily eroded surfaces that are re-colonised by new individuals of *S. nodosum* (NZ-171). (I) SEM image of a growth interruption (white arrow), with heavily abraded old cells in the lower right and initial cells of a new thallus growing towards the upper left (NZ-122).

Interior rhodolith composition analysis via µCT

Proportional interior compositions of the rhodoliths from the sandy subtidal (site 4, samples NZ-166, NZ-174), the rocky subtidal (site 5, samples NZ-106, NZ-109, NZ-126) and the beach supratidal (site 1, samples NZ-175, NZ-176, NZ-179, NZ-181, NZ-183) are visualised in Fig. 5A, indicating a similar distribution of the different organisms that built the skeletal matrix of the rhodoliths. This is confirmed by the PerMANOVA, which indicates no significant difference between samples from all sites ($F = 0.4949$, $P = 0.7494$). Exemplary µCT reconstructions showing specific organismal groups contributing to the overall rhodolith structure are depicted in Fig. 5B to G.

Petrographic analysis of lithoclastic rhodolith nuclei

Petrographic analysis revealed that both the rhodolith nuclei and the lithoclasts consisted of the volcanoclastic grit of the deformed Miocene flysch deposits prevailing at Army Bay. This material is characterised as a well-sorted, medium-grained sandstone rich in quartz. Proportional lithologic contents of the three rhodolith nuclei (NZ-154; NZ-171; NZ-192) and the two lithoclasts (NZ-Lith-1 and NZ-Lith-2) are visualised in Fig. 6A, indicating a similar distribution of the different components. The PerMANOVA indicates no significant difference between samples from both groups ($F = 2.414$, $P = 0.0693$), and characteristic lamination patterns are visible in all samples (Fig. 6B), making it very likely that rhodolith nuclei at and around Whangaparaoa derive from the adjacent cliffs at Army Bay.

Estimation of wave stress

Waves around Army Bay source mainly from the northern parts of the Hauraki Gulf, from the north-west in summer, autumn and early winter and from the north-east in late winter and

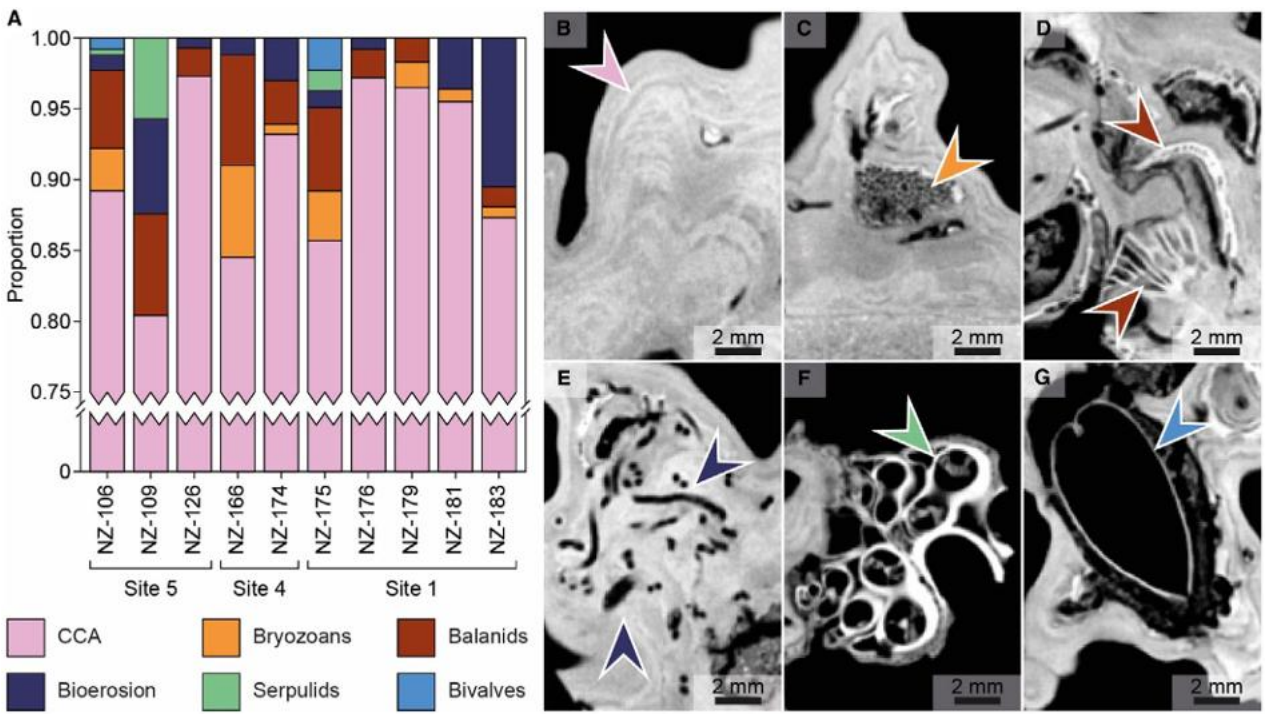

Fig. 5. Results of the rhodolith composition analysis via µCT. (A) Proportional composition of rhodolith builders and bioerosion from the sandy subtidal (site 4, samples NZ-166, NZ-174), the rocky subtidal (site 5, samples NZ-106, NZ-109, NZ-126) and the beach supratidal (site 1, samples NZ-175, NZ-176, NZ-179, NZ-181, NZ-183), indicating a similar distribution of the different groups; note adjustment of proportion axis for improved interpretability. (B) Crustose coralline algae (CCA). (C) Bryozoans. (D) Balanids. (E) Bioerosion. (F) Serpulids. (G) Boring bivalve.

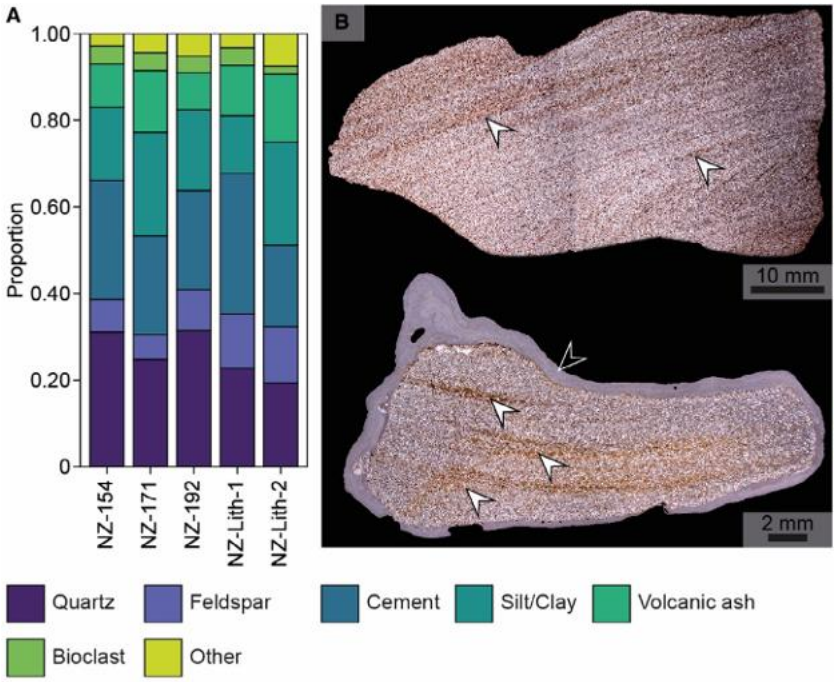

Fig. 6. Petrographic analysis of lithoclastic rhodolith nuclei. (A) Proportional lithologic contents of the three rhodolith nuclei (154; 171; NZ-192) and the two lithoclasts (NZ-Lith-1 and NZ-Lith-2), indicating a similar distribution of the different components. (B) Comparison of lithoclast NZ-Lith-1 and the CCA-coated grain NZ-192 (black arrow marks CCA coating) with the characteristic lamination patterns (white arrows) visible in both samples.

spring (Fig. 7A to C). Wave stress in Army Bay centres around late autumn to late winter, both with regard to ocean surface stress equivalent 10 m neutral wind speed and significant height of wind waves (Fig. 7D and E). Covering both main wave directions, the strong autumn and winter waves imply potential rhodolith transport directions from the sandy and rocky subtidal sites (sites 4 and 5, respectively) to the rocky intertidal of site 3 (the site described by Nalin *et al.* (2008) and Basso *et al.* (2009)) as well as to both supratidal sites (sites 1 and 2).

DISCUSSION

Rethinking rhodolith formation beyond classical bed models

Rhodoliths have long been associated with the development of laterally continuous, dense accumulations known as rhodolith beds, which serve as important sedimentary features and ecological habitats in marine carbonate systems (Aguirre *et al.*, 2017; Teichert, 2024). However, there remains no universally accepted definition of what constitutes a rhodolith bed, particularly with respect to coverage thresholds, percentage of live individuals or longevity of occupation (Bulleri *et al.*, 2025). In many systems, including those in the Mediterranean, South Pacific and South Atlantic, rhodolith beds are often interpreted as comparatively stable environments characterised by limited rhodolith redistribution and prolonged *in situ* growth (Bosence, 1983b; Tuya *et al.*, 2023), although rhodolith mobility and sedimentation rates may vary substantially between systems (Amado Filho *et al.*, 2012; Bracchi *et al.*, 2022).

In contrast, the present findings from Army Bay highlight a markedly different depositional configuration characterised by localised rhodolith growth, episodic redistribution and the apparent absence of a laterally continuous rhodolith bed sensu Steller *et al.* (2003) but rather form within confined rocky subtidal channels at around 5 m depth, where physical and biological conditions favour their growth. These rhodoliths are then redistributed landward, driven by storm-wave activity, into intertidal pools and supratidal beach zones (Fig. 8). Shallow-water rhodolith redistribution within tidal-channel

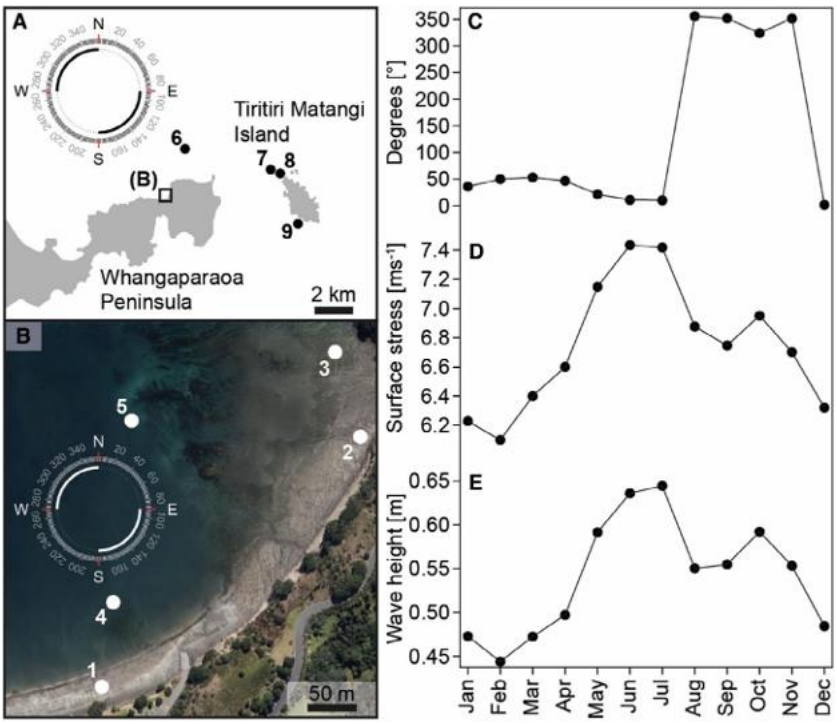

Fig. 7. Wave stress in the study area. (A) North-oriented overview on the complete study area, including the Whangaparaoa Peninsula and Tiritiri Matangi Island; numbered black dots indicate positions of scuba dive sampling spots (see also Table 1); area in the rectangle shown in D. (B) North-oriented satellite image (Courtesy of Google Inc.) of Army Bay; numbered white dots indicate snorkelling and hand collection sampling spots (see also Table 1). (C) Mean wave direction (source) over the course of the year, with two distinct main directions. (D) Wave stress expressed as ocean surface stress equivalent 10 m neutral wind speed. (E) Wave stress expressed as significant height of wind waves.

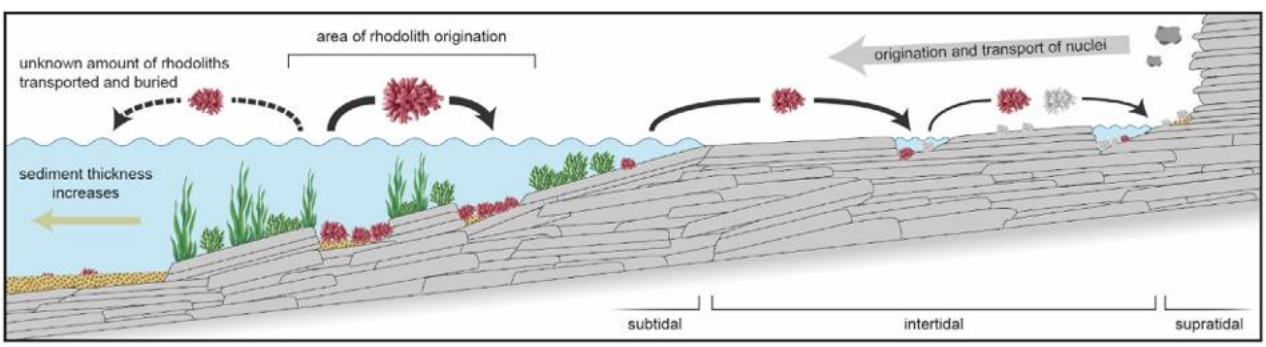

Fig. 8. Sedimentological model for rhodolith formation and transport at Army Bay, illustrating the spatial and dynamic relationships governing the formation, transport and deposition of *S. nodosum* rhodoliths in a shallow coastal setting. Lithoclastic nuclei originate from erosion of Miocene flysch cliffs and are transported downslope into the shallow rocky subtidal zone (~5 m depth), where erosional spur-and-groove-like structures act as sediment traps and hardground surfaces for rhodolith initiation. These lithologically inherited channels resemble coral reef spur-and-groove systems in function, with spurs colonised by macroalgae and crustose coralline algae, and grooves accumulating mobile rhodoliths. Rhodoliths grow concentrically in these channels, forming compact shapes. Living rhodoliths (red) are primarily found in these subtidal grooves, while dead, bleached specimens (white) accumulate in intertidal pools and supratidal beach zones. Seasonal storm-wave activity mobilises rhodoliths shoreward, selectively transporting smaller individuals due to their lower mass and entrainment threshold. Survival of offshore transport is limited due to the prevalence of mobile sandy substrates which cover transported rhodoliths quickly. This model challenges the classical rhodolith bed paradigm by demonstrating localised rhodolith genesis and episodic redistribution in the absence of extensive, laterally continuous accumulations.

environments has previously been documented by Bosellini & Ginsburg (1971), demonstrating that episodic hydrodynamic transport can significantly influence rhodolith accumulation patterns even over relatively small spatial scales.

This sedimentological and ecological dynamic expands current interpretations of rhodolith development, which have commonly emphasised stable and laterally extensive depositional settings. Instead of forming only in large, continuous beds under prolonged environmental stability, the results suggest that rhodolith communities can also thrive within more restricted, dynamic environments. In these narrow spatial corridors, rhodoliths maintain high carbonate productivity, but without necessarily developing into continuous, bed-like accumulations. Although direct long-term hydrodynamic monitoring was beyond the scope of this study, multiple independent observations—including rhodolith morphologies, abrasion patterns, redistribution gradients, wave-stress estimates and the distribution of living versus dead rhodoliths—consistently support episodic transport processes and fluctuating substrate conditions within the study area.

These findings are consistent with interpretations of fossil rhodolith-bearing limestones described by Nalin *et al.* (2008). In those deposits, rhodoliths are associated with transgressive systems, where rising sea levels created conditions of repeated disturbance. Rather than representing long-term, undisturbed growth, the rhodoliths in these successions often record repeated phases of transport, temporary burial, interruption of growth, surface abrasion and subsequent recolonisation. This pattern suggests that rhodolith assemblages can be resilient to environmental instability, repeatedly adapting to new substrates after being displaced by waves, currents or sediment influx.

Ultimately, the recognition that rhodolith systems can persist in such dynamic, corridor-like settings broadens the understanding of their ecological tolerance and depositional significance. Similar interpretations have previously been proposed for fossil rhodolith-bearing deposits associated with transgressive systems and storm-dominated shallow-marine environments (Johnson *et al.*, 2011). The Army Bay system provides a modern process-based example demonstrating how localised rhodolith production, episodic transport, growth interruption and repeated recolonisation may interact within a spatially restricted coastal setting. Consequently, fossil rhodolith assemblages may not always indicate large, stable carbonate factories, but may instead record episodes of environmental instability, shoreline migration or marine transgression.

Rocky subtidal sites as rhodolith production zones

Rhodolith formation is most prolific in the rocky subtidal zone (site 5), where erosional spur-and-groove-like channels carved into Miocene flysch deposits (Ballance, 1974; Spörli & Rowland, 2007) provide sheltered microhabitats and abundant lithoclastic nuclei. These channels act as natural sediment traps, offering a suitable environment for rhodolith accretion. The rhodoliths exhibit laminar to fruticose growth forms and signs of repeated abrasion and recolonisation, such as broken tips and internal growth interruptions, reflecting intermittent disturbance and exposure (Bosence, 1983a; Schlüter *et al.*, 2021). This environment functions analogously to spur-and-groove coral reef systems (Rogers *et al.*, 2015), although it is constructed purely from lithological architecture. The combination of hard substrate, moderate energy and sediment retention makes these subtidal zones the preferential rhodolith accumulation and growth environments of the system.

Transport and redistribution of rhodoliths: An onshore-directed pathway

Sphericities for the five Army Bay sites were very similar, while sizes and weights for the rocky supratidal rhodoliths (site 2) were much lower than for the rest (see also Fig. 3A), indicating that only small and/or light (less dense) rhodoliths are washed to the highest areas. Seasonal storm-wave activity, primarily during late autumn to winter (Fig. 7) appears to transport rhodoliths from subtidal channels landward into intertidal pools (site 3) and supratidal settings (sites 1 and 2). The hypothesis of an onshore-directed transport is supported by (1) decreasing rhodolith size and weight in supratidal areas, suggesting hydrodynamic sorting in which smaller and lighter rhodoliths are preferentially transported landward into supratidal depositional settings; (2) the presence of bleached, abraded rhodoliths in beach deposits; (3) morphological and compositional consistency across subtidal, intertidal and supratidal samples, supporting repeated redistribution within a

connected rhodolith system rather than the existence of distinct local populations. The observations of rhodolith redistribution at Army Bay parallel patterns described by Johnson *et al.* (2011) from the Middle Miocene of Madeira, where storm events were likewise identified as the primary driver of onshore rhodolith transport. In both cases, high-energy wave activity was capable of dislodging and mobilising rhodoliths from their production sites, moving them into more landward settings. At Ilhéu de Cima, hurricanes generated obrution deposits up to several meters thick, immobilising rhodoliths against volcanic topography. In contrast, at Army Bay, storms drive recurrent but small-scale transport from rocky subtidal channels into intertidal and supratidal zones, without producing laterally continuous, thick rhodolith beds. This difference likely reflects the restricted spatial extent of rhodolith production at Army Bay and the absence of an extensive offshore rhodolith accumulation that could supply large volumes of material for thick, laterally continuous storm deposits comparable to those described by Johnson *et al.* (2011).

Rhodoliths do not appear to be transported offshore into deeper waters (sites 6 to 9) in large numbers. Instead, rhodoliths found at these sites are sparse, thinly encrusted and show minimal signs of abrasion, indicating local, low-energy formation. This suggests that these offshore rhodoliths grow locally on isolated pebbles and cobbles within predominantly mobile sandy environments. Although offshore areas are likewise affected by storm activity, the extensive unconsolidated sand accumulations likely inhibit sustained rhodolith redistribution and preservation, because transported rhodoliths may rapidly become buried within the mobile sediment. In contrast, the nearshore Army Bay system contains rocky channel structures that facilitate repeated short-distance transport, trapping and reworking of rhodoliths within a spatially connected coastal corridor.

Lithoclastic provenance and local accretion

The nuclei of the *S. nodosum* rhodoliths from Army Bay are almost exclusively composed of well-sorted, volcaniclastic grit, petrographically indistinguishable from the Miocene flysch deposits exposed in the nearby coastal cliffs (Allen, 2004). The predominance of volcanoclastic grit nuclei throughout the investigated depositional settings supports the interpretation of a shared local lithoclastic source for the rhodolith system. This compositional match strongly supports a local, autochthonous origin of rhodolith nuclei and reinforces the conclusion that rhodolith formation is tied to the immediate geological setting.

This sedimentological linkage is significant for two reasons. Firstly, it implies that coastal erosion and cliff retreat directly drive rhodolith formation, supplying fresh lithoclasts that serve as primary hardground substrates. This tight coupling between terrestrial and shallow-marine sedimentary processes enhances the understanding of how dynamic coastal margins—particularly those in tectonically active regions like the Waitemata Basin (Spörli & Rowland, 2007)—can act as sources of carbonate sediment production via biogenic overgrowth of an originally siliciclastic setting. Second, the μCT analyses reveal that the internal composition of the rhodoliths—across all depositional settings—remains remarkably uniform. Biogenic constituents such as bryozoans, boring bivalves, serpulids and balanids are common and interspersed with CCA layers, regardless of whether the rhodoliths were collected from beach, intertidal or subtidal settings. This internal consistency, along with the absence of compositional gradients, suggests a relatively short turnover time between growth, transport and deposition. This supports the interpretation that rhodolith growth, transport and deposition within the Army Bay system are spatially interconnected, with many rhodoliths residing only briefly outside the preferential shallow subtidal growth environments before final burial or bleaching.

Palaeoecologically, the inclusion of encrusters and borers points to the role of rhodoliths as mobile microhabitats, even in high-energy systems. The rhodoliths host diverse associated calcifying, endolithic and bioeroding assemblages, consistent with the structurally complex habitats commonly described from rhodolith systems worldwide. Rhodolith beds are widely recognised as biodiversity-supporting habitats because their three-dimensional structure promotes habitat heterogeneity and provides ecological niches for diverse associated epifaunal, infaunal, endolithic, and cryptic communities (Steller *et al.*, 2003; Tuya *et al.*, 2023; Straube *et al.*, 2024), indicating that habitat function can persist even when the rhodoliths themselves are transient. From a fossil record perspective, this means that even scattered or reworked rhodoliths may preserve valuable biological and

ecological signals if internal structures are well-preserved (Basso *et al.*, 1998; Coletti *et al.*, 2015). Thus, Army Bay provides an important example of how localised lithoclastic supply, biological encrustation and hydrodynamic transport can interact to produce rhodoliths with complex but traceable sedimentological and ecological histories—all within a tightly constrained coastal system.

Implications for fossil rhodolith facies and shallow marine carbonate systems

This study presents a model where rhodolith development and accumulation are spatially decoupled, reflecting distinct environmental controls. Nearshore rhodoliths originate in shallow rocky zones and are transported landward during energetic events, while offshore rhodoliths form locally in calm, sand-dominated environments, isolated from shoreline inputs.

Such a system holds important implications for interpreting fossil rhodalgal facies. Mixed rhodolith deposits—particularly those showing variability in shape, abrasion and matrix composition—may represent composites of *in situ* and allochthonous components. Fossil analogues (Nalin *et al.*, 2008; Aguirre *et al.*, 2017) should be evaluated with caution, particularly in geologically active settings where sediment reworking and localised rhodolith production dominate. By expanding the concept of rhodolith accumulation beyond the classical 'bed' model, this study contributes to a more nuanced understanding of carbonate production and sediment transport dynamics in temperate shallow-marine systems, showing how rhodolith occurrence can be decoupled from the existence of a traditional bed and is instead linked to highly localised production zones and episodic transport processes.

ACKNOWLEDGEMENTS

The authors thank Christian Schulbert (FAU Erlangen-Nürnberg) for support with μCT scanning and data acquisition, and Birgit Leipner-Mata for preparation of thin sections. This research was funded by the Deutsche Forschungsgemeinschaft (DFG, German Research Foundation) under grant number 453305163. Open Access funding enabled and organized by Projekt DEAL.

CONFLICT OF INTERESTS

The authors declare no conflicts of interest.

DATA AVAILABILITY STATEMENT

The data that support the findings of this study are available from the corresponding author upon reasonable request.

REFERENCES

Aguirre, J., **Braga, J.C.** and **Bassi, D.** (2017) Rhodoliths and rhodolith beds in the rock record. In: *Rhodolith/Maërl Beds: A Global Perspective* (Eds Riosmena-Rodríguez, R., Nelson, W. and Aguirre, J.), pp. 105–138. Springer International Publishing, Cham.

Allen, S.R. (2004) The Parnell Grit beds revisited: are they all the products of sector collapse of western subaerial volcanoes of the Northland Volcanic Arc? *NZ J. Geol. Geophys.*, **47**, 509–524.

Amado Filho, G.M., **Moura, L.G.**, **Bastos, A.C.**, **Salgado, L.T.**, **Sumida, P.Y.**, **Guth, A.Z.**, **Francini-Filho, R.B.**, **Pereira Filho, G.H.**, **Abrantes, D.P.**, **Brasileiro, P.S.**, **Bahia, R.G.**, **Leal, R.N.**, **Kaufman, L.**, **Kleypas, J.A.**, **Farina, M.** and **Thompson, F.L.** (2012) Rhodolith beds are major $CaCO_3$ bio-factories in the tropical south west Atlantic. *PLoS One*, **7**, 35171.

Ballance, P.F. (1974) An inter-arc flysch basin in northern New Zealand: Waitemata Group (upper Oligocene to lower Miocene). *J. Geol.*, **82**, 439–471.

Basso, D., **Fravega, P.**, **Piazza, M.** and **Vannucci, G.** (1998) Biostratigraphic, paleobiogeographic and paleoecological implications in the taxonomic review of Corallinaceae. *Rend. Lincei*, **9**, 201–211.

Basso, D., **Nalin, R.** and **Nelson, C.S.** (2009) Shallow-water *Sporolithon* rhodoliths from North Island (New Zealand). *Palaios*, **24**, 92–103.

Basso, D., **Babbini, L.**, **Kaleb, S.**, **Bracchi, V.A.** and **Falace, A.** (2016) Monitoring deep Mediterranean rhodolith beds. *Aquat. Conserv. Mar. Freshw. Ecosyst.*, **26**, 549–561.

Bosellini, A. and **Ginsburg, R.N.** (1971) Form and internal structure of recent algal nodules (rhodolites) from Bermuda. *J. Geol.*, **79**, 669–682.

Bosence, D. (1976) Ecological studies on two unattached coralline algae from western Ireland. *Palaeontology*, **19**, 365–395.

Bosence, D. (1983a) Description and classification of rhodoliths (rhodoids, rhodolites). In: *Coated Grains* (Ed Peryt, T.M.), pp. 217–224. Springer, Berlin, Heidelberg.

Bosence, D. (1983b) The occurrence and ecology of recent rhodoliths—A review. In: *Coated Grains* (Ed Peryt, T.M.), pp. 225–242. Springer, Berlin, Heidelberg.

Bracchi, V.A., **Caronni, S.**, **Meroni, A.N.**, **Burguett, E.G.**, **Atzori, F.**, **Cadoni, N.**, **Marchese, F.** and **Basso, D.** (2022) Morphostructural characterization of the heterogeneous rhodolith bed at the marine protected area "capo carbonara" (Italy) and hydrodynamics. *Diversity*, **14**, 51.

Bulleri, F., **Schubert, N.**, **Hall-Spencer, J.M.**, **Basso, D.**, **Burdett, H.L.**, **Francini-Filho, R.B.**, **Grall, J.**, **Horta, P.A.**,

Kamenos, N.A., **Martin, S.**, **Nannini, M.**, **Neves, P.**, **Olive, I.**, **Pena, V.**, **Ragazzola, F.**, **Ribeiro, C.**, **Rinde, E.**, **Sissini, M.**, **Tuya, F.** and **Silva, J.** (2025) Positive species interactions structure rhodolith bed communities at a global scale. *Biol. Rev. Camb. Philos. Soc.*, **100**, 428–444.

Coletti, G., **Basso, D.**, **Frixa, A.** and **Corselli, C.** (2015) Transported rhodoliths witness the lost carbonate factory: a case history from the Miocene Pietra da Cantoni limestone (NW Italy). *Riv. Ital. Paleontol. Stratigr.*, **121**, 345–368.

Dean, A.J., **Steneck, R.S.**, **Tager, D.** and **Pandolfi, J.M.** (2015) Distribution, abundance and diversity of crustose coralline algae on the Great Barrier Reef. *Coral Reefs*, **34**, 581–594.

Demirmen, F. (1971) Counting error in petrographic point-count analysis: a theoretical and experimental study. *J. Int. Assoc. Math. Geol.*, **3**, 15–41.

Flügel, E. (2010) *Microfacies of Carboate Rocks—Analysis, Interpretation and Application*. Springer, Berlin, Heidelberg.

Foster, M.S. (2001) Rhodoliths: between rocks and soft places. *J. Phycol.*, **37**, 659–667.

Gabrielson, P.W., **Hughey, J.R.**, **Peña, V.**, **Richards, J.L.**, **Saunders, G.W.**, **Twist, B.**, **Farr, T.** and **Nelson, W.A.** (2023) Asia Pacific *Sporolithon* (Corallinophycidae, Rhodophyta) species revised based on DNA sequencing of type specimens and including *S. crypticum* sp. nov., *S. immotum* sp. nov. and *S. nodosum* sp. nov. *Phycologia*, **62**, 1–15.

Gorman, R.M., **Bryan, K.R.** and **Laing, A.K.** (2003) Wave hindcast for the New Zealand region: nearshore validation and coastal wave climate. *NZ J. Mar. Freshw. Res.*, **37**, 567–588.

Graham, D.J. and **Midgley, N.G.** (2000) Graphical representation of particle shape using triangular diagrams: an Excel spreadsheet method. *Earth Surf. Proc. Land.*, **25**, 1473–1477.

Hersbach, H., **Bell, B.**, **Berrisford, P.**, **Hirahara, S.**, **Horányi, A.**, **Muñoz-Sabater, J.**, **Nicolas, J.**, **Peubey, C.**, **Radu, R.**, **Schepers, D.**, **Simmons, A.**, **Soci, C.**, **Abdalla, S.**, **Abellan, X.**, **Balsamo, G.**, **Bechtold, P.**, **Biavati, G.**, **Bidlot, J.**, **Bonavita, M.**, **De Chiara, G.**, **Dahlgren, P.**, **Dee, D.**, **Diamantakis, M.**, **Dragani, R.**, **Flemming, J.**, **Forbes, R.**, **Fuentes, M.**, **Geer, A.**, **Haimberger, L.**, **Healy, S.**, **Hogan, R.J.**, **Hólm, E.**, **Janisková, M.**, **Keeley, S.**, **Laloyaux, P.**, **Lopez, P.**, **Lupu, C.**, **Radnoti, G.**, **de Rosnay, P.**, **Rozum, I.**, **Vamborg, F.**, **Villaume, S.** and **Thépaut, J.-N.** (2020) The ERA5 global reanalysis. *Q. J. Roy. Meteorol. Soc.*, **146**, 1999–2049.

Johnson, M.E., **da Silva, C.M.**, **Santos, A.**, **Baarli, B.G.**, **Cachão, M.**, **Mayoral, E.J.**, **Rebelo, A.C.** and **Ledesma-Vázquez, J.** (2011) Rhodolith transport and immobilization on a volcanically active rocky shore: Middle Miocene at Cabeço das Laranjas on Ilhéu de Cima (Madeira Archipelago, Portugal). *Palaeogeogr. Palaeoclimatol. Palaeoecol.*, **300**, 113–127.

Kamenos, N.A., **Moore, P.G.** and **Hall-Spencer, J.M.** (2004) Nursery-area function of maerl grounds for juvenile queen scallops *Aequipecten opercularis* and other invertebrates. *Mar. Ecol. Prog. Ser.*, **274**, 183–189.

Littler, M.M., **Littler, D.S.**, **Blair, S.M.** and **Norris, J.N.** (1985) Deepest known plant life discovered on an uncharted seamount. *Science*, **227**, 57–59.

López Correa, M., **Teichert, S.**, **Ragazzola, F.**, **Cazorla Vázquez, S.**, **Engel, F.B.**, **Hurle, K.**, **Mazzoli, C.**, **Kuklinski, P.**, **Raiteri, G.** and **Lombardi, C.** (2023) Structural and geochemical assessment of the coralline alga *Tethysphytum antarcticum* from Terra Nova Bay, Ross Sea, Antarctica. *Minerals*, **13**, 215.

Nalin, R., **Nelson, C.S.**, **Basso, D.** and **Massari, F.** (2008) Rhodolith-bearing limestones as transgressive marker beds: fossil and modern examples from North Island, New Zealand. *Sedimentology*, **55**, 249–274.

OSPAR. (2008) Case reports for the OSPAR list of threatened and/or declining species and habitats.

Pardo, C., **Guillemin, M.-L.**, **Peña, V.**, **Bárbara, I.**, **Valero, M.** and **Barreiro, R.** (2019) Local coastal configuration rather than latitudinal gradient shape clonal diversity and genetic structure of Phymatolithon calcareum Maerl Beds in North European Atlantic. *Front. Mar. Sci.*, **6**, 149.

Pyko, I., **Wisshak, M.** and **Teichert, S.** (2025) Depth-related controls on the quantitative composition of rhodolith matrices in the high Arctic. *Aquat. Conserv.*, **35**, e70045.

Ragazzola, F., **Kolzenburg, R.**, **Zekonyte, J.**, **Teichert, S.**, **Jiang, C.**, **Zuljevic, A.**, **Caragnano, A.** and **Falace, A.** (2020) Structural and elemental analysis of the freshwater, low-Mg calcite coralline alga *Pneophyllum cetinaensis*. *Plants*, **9**, 1089.

Richmond, R.H. and **Hunter, C.L.** (1990) Reproduction and recruitment of corals: comparisons among the Caribbean, the Tropical Pacific, and the Red Sea. *Mar. Ecol. Prog. Ser.*, **60**, 185–203.

Riding, R., **Cope, J.C.W.** and **Taylor, P.D.** (1998) A coralline-like red alga from the lower Ordovician of Wales. *Palaeontology*, **41**, 1069–1076.

Rinde, E., **Moy, S.R.**, **Tveiten, L.A.**, **Kvile, K.Ø.**, **Walday, M.G.**, **Christie, H.C.**, **Brkljacic, M.S.**, **Kile, M.R.**, **Bekkby, T.**, **Gitmark, J.K.**, **Mjelde, M.**, **Fagerli, C.W.**, **Oug, E.** and **d'Auriac, M.A.** (2022) Feltbasert kunnskap, metodikk og kriterier for økologisk kvalitet til et utvalg av marine naturtyper.

Rogers, J.S., **Monismith, S.G.**, **Dunbar, R.B.** and **Koweek, D.** (2015) Field observations of wave-driven circulation over spur and groove formations on a coral reef. *J. Geophys. Res. Oceans*, **120**, 145–160.

Schlüter, M., **Pyko, I.**, **Wisshak, M.**, **Schulbert, C.** and **Teichert, S.** (2021) Growth interruptions in Arctic rhodoliths correspond to water depth and rhodolith morphology. *Minerals*, **11**, 538.

Sneed, E.D. and **Folk, R.L.** (1958) Pebbles in the lower Colorado river, Texas. A study in particle morphogenesis. *J. Geol.*, **66**, 114–150.

Spörli, K.B. and **Rowland, J.V.** (2007) Superposed deformation in turbidites and syn-sedimentary slides of the tectonically active Miocene Waitemata Basin, northern New Zealand. *Basin Res.*, **19**, 199–216.

Steller, D.L., **Riosmena-Rodríguez, R.**, **Foster, M.S.** and **Roberts, C.A.** (2003) Rhodolith bed diversity in the Gulf of California: the importance of rhodolith structure and consequences of disturbance. *Aquat. Conserv.*, **13**, S5–S20.

Steneck, R.S. (1986) The ecology of coralline algal crusts: convergent patterns and adaptive strategies. *Annu. Rev. Ecol. Syst.*, **17**, 273–303.

Straube, E., **Neumann, H.**, **Wisshak, M.**, **Mathes, G.** and **Teichert, S.** (2024) Bayesian analysis of biodiversity patterns via beam trawl versus video transect—a comparative case study of Svalbard rhodolith beds. *Biodivers. Conserv.*, **33**, 1099–1123.

Tâmega, F.T.S., **Grimaldi, G.**, **Macedo, A.**, **Barbosa, S.O.**, **Anderson, A.B.**, **Bastos, E.**, **Freire, V.**, **Moreira, A.**, **Fernandes, C.**, **Figueiredo, M.A.O.**, **Carneiro, P.B.**, **Gouvêa, L.P.** and **Horta, P.A.** (2024) Biodiversity

associated with rhodolith beds in Brazil. In: *Brazilian Rhodolith Beds: Oasis of Marine Biodiversity to be Protected* (Eds Horta, P.A. and Sissini, M.N.), pp. 67–103. Springer Nature, Cham.

Teichert, S. (2014) Hollow rhodoliths increase Svalbard's shelf biodiversity. *Sci. Rep.*, **4**, 6972.

Teichert, S. (2024) Attached and free-living crustose coralline algae and their functional traits in the geological record and today. *Facies*, **70**, 27.

Teichert, S., **Woelkerling, W.** and **Munnecke, A.** (2019) Coralline red algae from the Silurian of Gotland indicate that the order Corallinales (Corallinophycidae, Rhodophyta) is much older than previously thought. *Palaeontology*, **62**, 599–613.

Teichert, S., **Reddin, C.J.** and **Wisshak, M.** (2024) In situ decrease in rhodolith growth associated with Arctic climate change. *Glob. Chang. Biol.*, **30**, e17300.

Tuya, F., **Schubert, N.**, **Aguirre, J.**, **Basso, D.**, **Bastos, E.O.**, **Berchez, F.**, **Bernardino, A.F.**, **Bosch, N.E.**, **Burdett, H.L.**, **Espino, F.**, **Fernández-Gárcia, C.**, **Francini-Filho, R.B.**, **Gagnon, P.**, **Hall-Spencer, J.M.**, **Haroun, R.**, **Hofmann, L.C.**, **Horta, P.A.**, **Kamenos, N.A.**, **Le Gall, L.**, **Magris, R.A.**, **Martin, S.**, **Nelson, W.A.**, **Neves, P.**, **Olivé, I.**, **Otero-Ferrer, F.**, **Peña, V.**, **Pereira-Filho, G.H.**, **Ragazzola, F.**, **Rebelo, A.C.**, **Ribeiro, C.**, **Rinde, E.**, **Schoenrock, K.**, **Silva, J.**, **Sissini, M.N.** and **Tâmega, F.T.S.** (2023) Levelling-up rhodolith-bed science to address global-scale conservation challenges. *Sci. Total Environ.*, **892**, 164818.

Walters, R.A., **Goring, D.G.** and **Bell, R.G.** (2001) Ocean tides around New Zealand. *NZ J. Mar. Freshw. Res.*, **35**, 567–579.

Žuljević, A., **Kaleb, S.**, **Peña, V.**, **Despalatović, M.**, **Cvitković, I.**, **De Clerck, O.**, **Le Gall, L.**, **Falace, A.**, **Vita, F.**, **Braga, J.C.** and **Antolić, B.** (2016) First freshwater coralline alga and the role of local features in a major biome transition. *Sci. Rep.*, **6**, 19642.

Manuscript received 11 September 2025; revision accepted 2 August 2026